PAPER

Role of the caudal peduncle in a fish-inspired robotic model: how changing stiffness and angle of attack affects swimming performance

To cite this article: David G Matthews *et al* 2022 *Bioinspir. Biomim.* **17** 066017

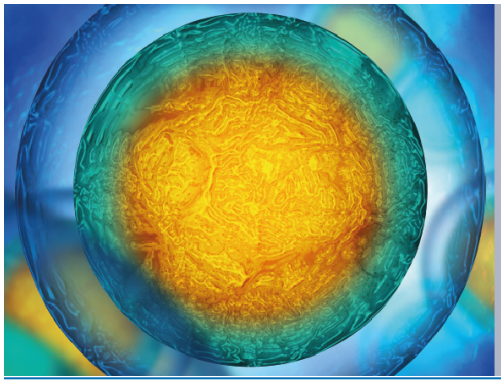

IOP Publishing Bioinspir. Biomim. 17 (2022) 066017 https://doi.org/10.1088/1748-3190/ac9879

Bioinspiration & Biomimetics

PAPER

RECEIVED
5 May 2022

REVISED
22 September 2022

ACCEPTED FOR PUBLICATION
6 October 2022

PUBLISHED
31 October 2022

Role of the caudal peduncle in a fish-inspired robotic model: how changing stiffness and angle of attack affects swimming performance

David G Matthews[1,2,4,*], Ruijie Zhu[3,4], Junshi Wang[3,5], Haibo Dong[3], Hilary Bart-Smith[3] and George Lauder[1,2]

[1] Department of Organismic and Evolutionary Biology, Harvard University, Cambridge, MA 20138, United States of America
[2] Museum of Comparative Zoology, Harvard University, Cambridge, MA 20138, United States of America
[3] Department of Mechanical & Aerospace Engineering, University of Virginia, Charlottesville, VA 22904, United States of America
[4] These authors contributed equally to this work.
[5] Present address: Department of Mechanical and Aerospace Engineering, Princeton University, Princeton, NJ 08544, United States of America.
[*] Author to whom any correspondence should be addressed.

E-mail: matthewswehttam@gmail.com

Keywords: fish, robot, foil, stiffness, locomotion

Supplementary material for this article is available online

Abstract

In fish, the tail is a key element of propulsive anatomy that contributes to thrust during swimming. Fish possess the ability to alter tail stiffness, surface area and conformation. Specifically, the region at the base of the tail, the caudal peduncle, is proposed to be a key location of fish stiffness modulation during locomotion. Most previous analyses have focused on the overall body or tail stiffness, and not on the effects of changing stiffness specifically at the base of the tail in fish and robotic models. We used both computational fluid dynamics analysis and experimental measurements of propulsive forces in physical models with different peduncle stiffnesses to analyze the effect of altering stiffness on the tail angle of attack and propulsive force and efficiency. By changing the motion program input to the tail, we were able to alter the phase relationship between the front and back tail sections between 0° and 330°. Computational simulations showed that power consumption was nearly minimized and thrust production was nearly maximized at the kinematic pattern where $\phi = 270°$, the approximate phase lag observed in the experimental foils and in free swimming tuna. We observed reduced thrust and efficiency at high angles of attack, suggesting that the tail driven during these motion programs experiences stalling and loss of lift. However, there is no single peduncle stiffness that consistently maximizes performance, particularly in physical models. This result highlights the fact that the optimal caudal peduncle stiffness is highly context dependent. Therefore, incorporating the ability to control peduncle stiffness in future robotic models of fish propulsion promises to increase the ability of robots to approach the performance of fish.

1. Introduction

Engineers and biologists alike have long been fascinated by the high performance and efficiency with which fish such as tuna are able to swim. One reason for the high level of locomotor performance acheived by fish is their ability to manipulate the movement and material properties of their body and fins, reviewed most recently by Quinn and Lauder [1]. Most analyses have focused on changing body stiffness [2–5] and on how fish can actively adjust fin ray stiffness [6–8] during swimming. However, motor control of the tail and its stiffness modulation is also of considerable interest [9, 10]. Research on the motor control of fish tails has recently begun to focus on the caudal peduncle, the portion of the tail that connects the body to the caudal fin (figures 1(A) and (B)). In fish, this anatomical region contains tendons from the body's musculature that connect to tail fin rays, and there is often considerable modification of the

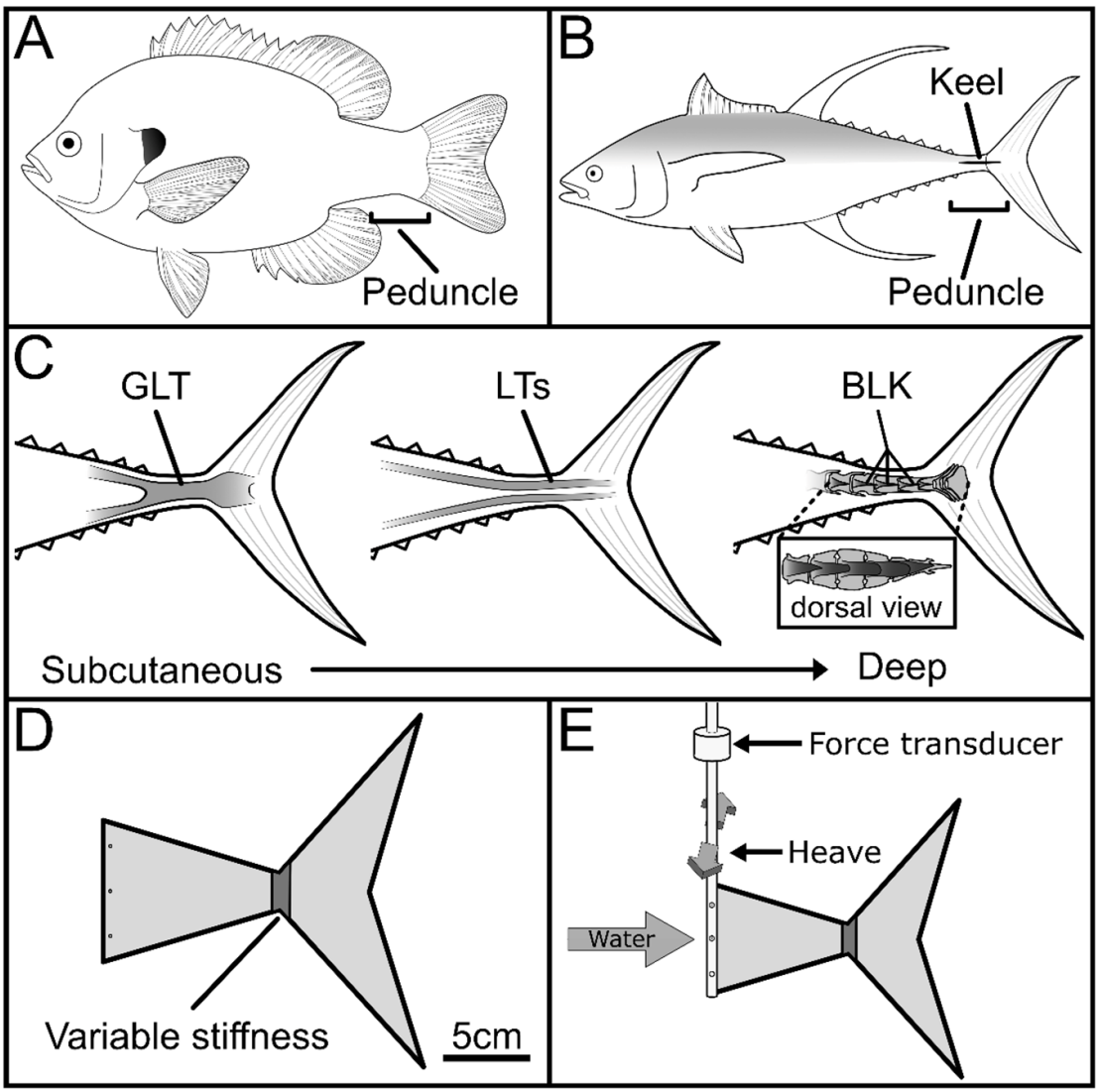

Figure 1. Experimental foils designed to reflect the anatomy and variable stiffness of fish tails. (A) The peduncle region of percomorph fishes, such as a bluegill (*Lepomis macrochirus*), is relatively deep. (B) The peduncle region of many scombrid fishes, such as a yellowfin tuna (*Thunnus albacares*), is narrow and has a specialized keel structure with a visible external portion composed of collagenous tissue. (C) Internal anatomy of a tuna tail showing the layers of tissue that passively stiffen the peduncle. Most distal from the midline is the great lateral tendon (GLT). Medial to the GLT are the lateral tendons (LTs). At the midline there is a bony lateral keel (BLK) formed from interlocking lateral projections from peduncle vertebrae. (D) Experiments were carried out on foils whose geometry is inspired by the tuna tail, with variable stiffness provided by changing the material composition at the peduncle. (E) Recirculating flow tank experiments were performed by actuating bioinspired foils in heave and allowing the peduncle joint to control the pitching motion of the caudal fin. Resultant forces were measured using an in-line force transducer. Further details of the foils and testing apparatus are provided in supplemental figures 1 and 2.

vertebrae anterior to the bony supports of the tail fin rays (figure 1(C); [11, 12]). Antagonistic activation of body musculature can stiffen the tendons attached to the tail, and similar antagonistic activation of the caudal fin musculature can stiffen the tail fin rays (reviewed in [1]). Recent experimental studies using mechanical systems to model the caudal peduncle include the work of Ren *et al* [13], who found that active pitching of the caudal fin using the peduncle could improve lift, thrust and maneuverability compared to a heave-only caudal fin. More recently, Zhong *et al* [14] found that active tensioning of the peduncle region allowed swimming fish models to maximize efficiency across a range of swimming speeds by modulating stiffness. Additionally, some of the highest performance swimming robots to date have incorporated fish-like caudal peduncles as an integral part of their design [15, 16]. Despite this increased focus on the role of the caudal peduncle region for efficient swimming, the mechanisms by which the peduncle affects tail hydrodynamics and the extent to which changes in stiffness at the base of the tail alter swimming thrust and efficiency are not known.

During steady swimming, the caudal fin of fish moves in two primary axes, laterally perpendicular to the flow (heave), and rotationally about the peduncle joint (pitch) [17]. The fish caudal peduncle region is involved in generating both types of motion. Specifically, the peduncle transmits the lateral force generated by the body muscles to the caudal fin allowing it to

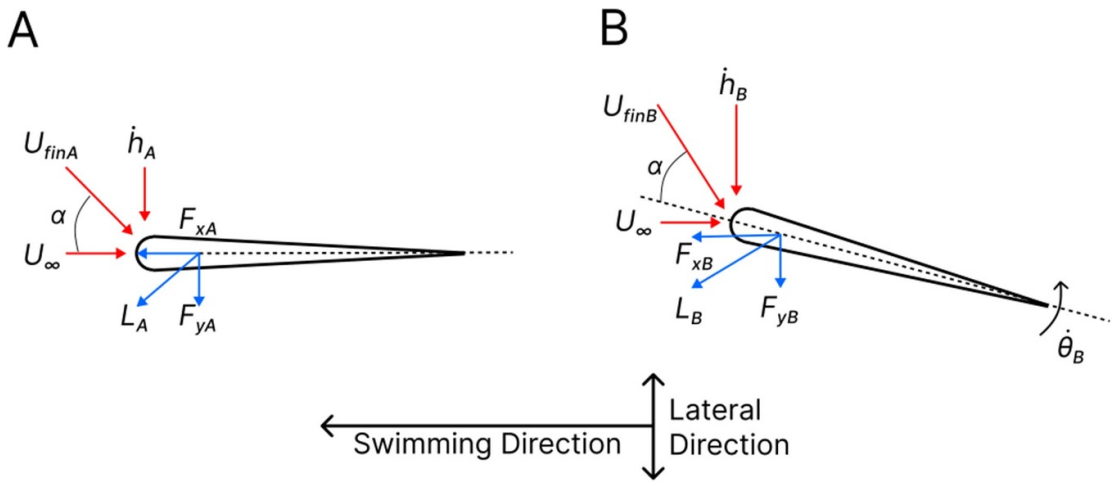

Figure 2. The addition of pitch (B) to a heave-only motion pattern (A) allows for greater lift generation without inducing dynamic stall. (A) Free-stream flow (U_∞) combined with heave motion ($\dot{h}_A$) generates the effective fin velocity (U_A). Lift (L_A) is generated perpendicular to the effective fin velocity, and the streamwise component (F_{xA}) of this force is considered thrust. However, as $\dot{h}_A$ increases the angle of attack (α) quickly increases and surpasses the stall point of the system. (B) By including a pitching motion $\dot{\theta}_B$ in addition to heave, the angle of attack can be reduced for the same heave motion, thereby allowing for higher effective fin velocities before exceeding the stall point.

move in heave. As the fin moves laterally through the water, the stiffness of the peduncle then determines the degree to which the fin is deflected, thereby affecting the maximum pitch of the fin. Additionally, fish can use active muscle contraction to alter the relative timing of heave motion and to stiffen the peduncle for additional alteration of pitching motion. There has been much speculation that fish actively modulate the stiffness of the tail in this way, but there is little evidence of this or that they substantially change the timing of caudal fin heaving motion through active muscle contractions in the peduncle [1, 9, 18, 19]. Rather, the timing of the caudal fin relative to the body generally appears to be consistent with a model in which a mostly passive fin is actuated at its leading edge.

As fish undulate their tails, thrust is generated through several mechanisms including lift on the caudal fin. Lift-based locomotion can be highly efficient [20–22] but is dependent on optimizing the motion of the tail relative to the water around it. As the tail moves to the side during undulatory propulsion, the lateral velocity $\dot{h}_A$ interacts with freestream velocity U_∞ into an effective net fin velocity U_{finA} that produces lift L_A (figure 2(A)). The lift vector is perpendicular to U_{finA}, L_A has orthogonal components in the lateral and swimming directions (F_{yA} and F_{xA}, respectively), with the latter considered thrust.

To produce thrust efficiently, fish must avoid dynamic stalling of the caudal fin, and thus need to limit the maximum angle of attack, α. However, to increase thrust, the tail must increase in frequency and the resulting lateral heave velocity, which will then increase the angle of attack. This conflict between thrust and efficiency can be mitigated by adding a pitch motion $\dot{\theta}_B$ with an appropriate phase offset ϕ to the heave motion such that the angle of attack is reduced (figure 2(B)). Similar mechanisms have been studied in flat foils with a wide range of Reynolds numbers [23, 24]. The lateral velocity of the fin is greater than in a heave-only motion, but the angle of attack does not increase due to the addition of appropriate pitch $\dot{\theta}_B$. Increased heave velocity $\dot{h}_B$ increases the lift L_B and rotates the resultant force vector into the thrust (F_{xB}) direction, increasing overall efficiency η. Thus, the phase offset ϕ between the heave and pitch motions of the caudal fin is a crucial factor in determining the propulsive performance of an undulatory swimmer.

In this study, we seek to further elucidate the role of the caudal peduncle in optimizing swimming performance metrics, including thrust production, power consumption and Froude efficiency, by examining its role in mediating the relative motion of the body and the tail in the context of lift-based locomotion. We do this through a combination of simulations and experiments on a bioinspired tuna-shaped tail. We first computationally investigate the optimal phase offset between the body and the tail to see if greater active input from the caudal peduncle to phase advance the caudal fin can increase swimming performance. We apply these results in the context of flow over the caudal fin to understand whether the results can be explained by our understanding of lift generation. We then experimentally examine the energetics of swimming in physical models with different caudal peduncle stiffnesses, allowing for different pitching amplitudes of the caudal fin. We hypothesize that the primary benefit to be gleaned from the peduncle is through modulation of the angle of attack of the fin and not through modulation of the relative timing of tail heaving motion.

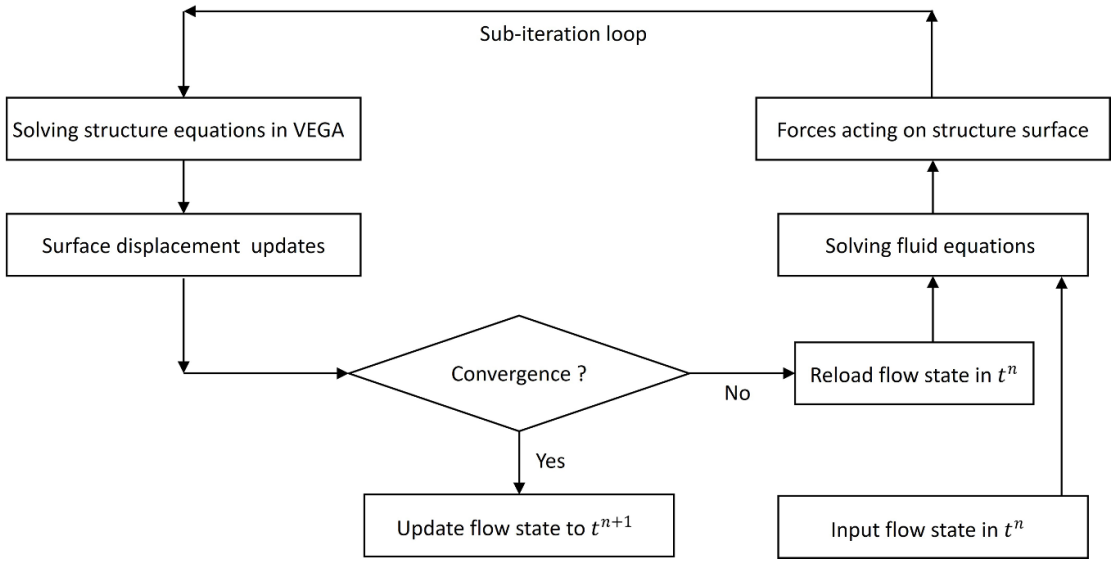

Figure 3. Schematic overview of the fluid–structure interaction solver workflow. t^n is the nth time step.

2. Methods

2.1. Computational fluid modeling

We coupled an in-house immersed boundary method based flow solver Picar3D [25] and an open-source finite element structure solver (Vega finite element modeling (FEM), University of Southern California, Los Angeles, CA) [26] to perform fluid–structure interaction (FSI) simulations. During this process, the convergence check guarantees the convergence of the flow and structure results at each time iteration, allowing us to achieve strong coupling between the fluid solver and the structure solver (figure 3). Recently, the FSI solver was successfully applied to study the hydrodynamic performance of a flexible tuna tail [27].

The fluid solver solves the incompressible Navier–Stokes equations, which are non-dimensionalized by chord length and incoming flow speed. We solve these equations numerically using an in-house finite-difference-based Cartesian-grid sharp-interface immersed-boundary-method direct numerical simulation solver [25]. This approach has been successfully applied to the flapping propulsion of insects [28–30], birds [31, 32], fish [33–35], as well as various biological and bioinspired problems [36–38]. A detailed description of the sharp-interface method and validation of this solver can be found in [39, 40]. The structure solver uses the open-source Vega FEM Library, chosen for its ability to handle large deformations [26]. The solver numerically solves an ordinary differential equation derived from finite element analysis. A more detailed description of the coupled numerical algorithms is provided in Wang *et al* [41].

We model a foil (same shape as shown in figure 1(D) and supplemental figure 1, one-half dimension) inspired by a tuna tail, and use a computational domain with non-uniform density to calculate fluid motion (figure 4(A)). In the current simulations, we first perform a fully prescribed setup where both the body (section anterior to peduncle) and the caudal fin (section posterior to peduncle) are rigid and have prescribed motions (figure 4(B)). We then perform an FSI setup where the caudal fin is connected to the prescribed body through a flexible peduncle (supplemental figure 1).

For the full prescribed setup, the section of the foil anterior to the peduncle is driven with prescribed sinusoidal heave motion of amplitude $h_0 = 0.0125$ m. The tail section posterior to the peduncle has the same heave motion but is also driven by a pitching motion of amplitude $\theta_0 = 15°$. For the posterior part, pitching and heaving both have the same frequency of $f = 1$ Hz, but are phase offset from the body by $\phi = 0°$–$330°$. Phase offsets are prescribed in intervals of 90° between 0° and 180°, with a more refined spacing of 30° between 210° and 330° (table 1). We sampled more cases between 210° and 330° because we expected the most biomimetic kinematic profiles to fall within this range. In total, the parameter space has 24 different simulation cases. The representative kinematics of the foils are shown in figure 5.

For each of the 24 simulation cases we calculate the mean streamwise force (F_x) and lateral force (F_y) over the duration of one complete flapping cycle. We then use the force data to calculate key swimming performance metrics, including the coefficient of thrust, coefficient of power and Froude efficiency (equations (1)–(3)) for each set of trials, where s is

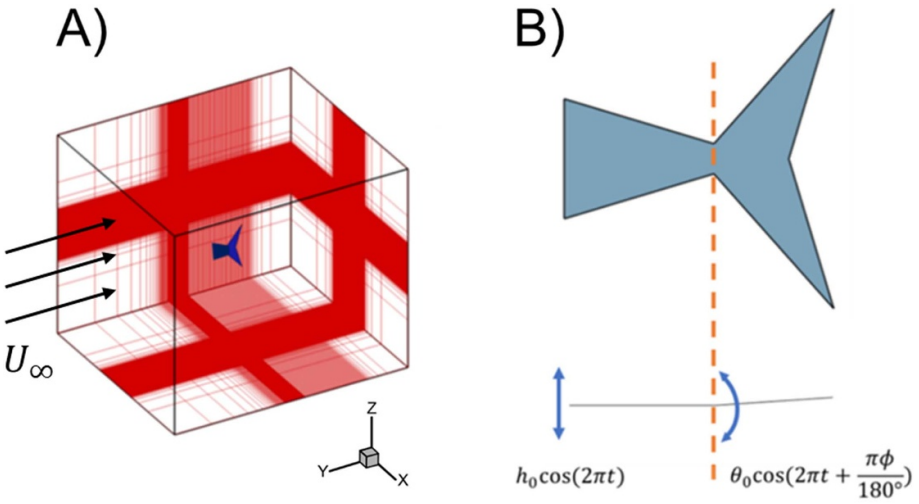

Figure 4. Computational fluid dynamic (CFD) simulation design showing (A) CFD mesh arrangement and (B) equations determining foil kinematics in both heave and pitch. The equation on the left represents the motion anterior to the peduncle and the equation on the right represents motion posterior to the peduncle. U_∞ represents free-stream velocity.

Table 1. Simulation parameters for analyzing the effect of phase offsets on propulsion.

Parameter	Range
Free-stream velocity	$U_\infty = 0.08, 0.12, 0.16$ m s^{-1}
Chord	$c = 0.09$ m (body $c_1 = 0.05$ m, fin $c_2 = 0.04$ m)
Span	$s = 0.1$ m
Frequency	$f = 1$ Hz
Heave amplitude	$h_0 = 0.0125$ m
Bend angle	$\theta_0 = 15^\circ$
Phase offset	$\phi = 0^\circ, 90^\circ, 180^\circ, 210^\circ, 240^\circ, 270^\circ, 300^\circ, 330^\circ$

the foil span, c is the foil chord, U_∞ is the free-stream velocity, h is the heaving amplitude and ρ is the density of water at 20 °C:

$$C_T = \frac{F_x}{\frac{1}{2}\rho U_\infty^2 sc}, \quad (1)$$

$$C_P = \frac{F_y \dot{h}}{\frac{1}{2}\rho U_\infty^3 sc}, \quad (2)$$

$$\eta = \frac{C_T}{C_P}. \quad (3)$$

To supplement the force data, we calculated the Strouhal number as well as the angle of attack throughout a complete oscillatory cycle (equations (4) and (5)), where f is the frequency of motion and $c_2 \sin\theta \cos\phi$ represents the position of the tail relative to the actuated leading edge. We then recorded the maximum angle of attack for each foil at any point during the flapping cycle and used this value in our analyses:

$$\mathrm{St} = \frac{2f(h + c_2 \sin\theta \cos\phi)}{U_\infty}, \quad (4)$$

$$\alpha = -\theta - \tan^{-1}\left(\frac{h}{U_\infty}\right). \quad (5)$$

2.2. Foil design and manufacture

Simulation results suggested that passive bending at the caudal peduncle optimized several performance variables, so we continued our investigation by manufacturing plastic foils with flexible peduncle joints. Each foil was manufactured with a Stratasys object printer (0.03 mm layer resolution) with the same shape as the computational model (figure 1(D), supplemental figure 1), but we varied the stiffness at the peduncle by altering material thickness. Specifically, each foil is composed of three UV cured polymer (VeroWhite by Stratasys) layers on the body and tail with only the central layer spanning the peduncle joint. The thickness of this central layer directly determines the stiffness of the peduncle and therefore the bending angle of the tail as the leading edge of the foil is actuated in heave. We kept the overall thickness of the foil uniform by filling the peduncle region with a rubber-like material (TangoBlack by Stratasys).

To ensure a wide distribution of experimental peduncle stiffnesses in our tuna-inspired foils, we conducted three-point bending tests across a range of peduncle material thicknesses to measure the flexural modulus of the tri-laminar structure (supplemental figure 2). The rectangular specimens used for bending tests had a span of 60 mm, chord of 20 mm and thickness of 2 mm. Similar to the peduncle joint on experimental foils, these specimens were composed of one central polymer layer of variable thickness and two rubber layers to bring the total thickness to 2 mm. The central layer varied in thickness from 7 to 2 mm, with three specimens manufactured for each set of specifications to allow trial replication. We calculate the flexural modulus using equation (6), where L is the span between the supports, m is the slope of the

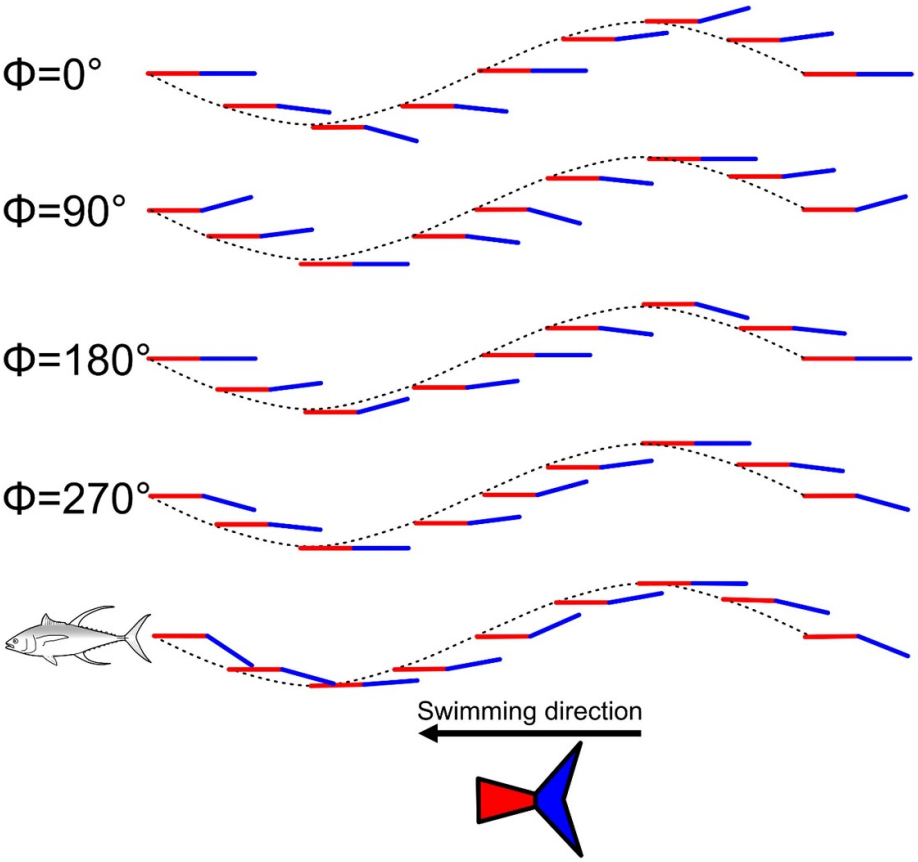

Figure 5. Prescribed kinematics of simulated foils at four representative phase values compared to data from a freely swimming yellowfin tuna obtained from high-speed video recordings of free-swimming tuna locomotion. Blue denotes the portion of the tail posterior to the peduncle while red denotes the tail segment anterior to the peduncle. Tuna kinematic traces were aligned to keep the red segment parallel.

Table 2. Experimental foil design parameters.

Foil	Peduncle thickness (m)	Stiffness at center of peduncle, EI (Pa m^4)
S1	3.0×10^{-4}	1.35×10^{-3}
S2	5.0×10^{-4}	6.24×10^{-3}
S3	7.0×10^{-4}	1.71×10^{-2}
S4	1.0×10^{-3}	4.99×10^{-2}

linear portion of the deflection curve, b is the width of the foil and d is the thickness of the foil:

$$E_f = \frac{L^3 m}{4bd^3}. \quad (6)$$

Finally, we fit a cubic function to the plot of flexural modulus against foil thickness and use this to choose four thicknesses of experimental foils (table 2).

2.3. Flow tank experiments and PIV

We conducted experiments using a robotic system capable of actuating the foils in heave at the leading edge (figure 1(E); supplemental figures 1 and 3; video 1) (see [42–46] for further details of this experimental platform). We suspended this system over a recirculating flow tank with the foil held in the water by a flat shaft. We measured the forces using a six-axis force-torque transducer (ATI-Nano 17, ATI Industrial Automation, Apex, NC, USA) at the top of the shaft. During each experimental trial, we placed the foil in a flow tank with a free stream velocity of 0.24 m s^{-1} and actuated the foil for 10 s while recording raw force data (F_x and F_y), then measured the mean values calculated over the entire flapping period. We ran five trials for each foil while varying the frequency of motion and heave amplitude of the leading edge (table 3) before calculating the mean and standard deviations across the trials using R language (R v.3.5.3, RStudio v1.0.153). We did not complete trials at high heave and high frequencies for the most flexible foils because the printed peduncle joint was not strong enough to withstand the actuation forces. Finally, we used the force data to measure the coefficient of thrust, power consumption and Froude efficiency (equations (1)–(3)).

To understand whether our experimentally measured flow patterns were similar to the simulation results, we recorded flow around the foils during one trial at each combination of foil and kinematic parameters. Flow was captured from a ventral view via

Table 3. Experimental parameters used for the flow tank experiments.

Parameter	Range
Free-stream velocity	$U_\infty = 0.24$ m s^{-1}
Chord	$c = 0.18$ m (body $c_1 = 0.1$ m, fin $c_2 = 0.08$ m)
Span	$s = 0.2$ m
Frequency	$f = 0.4, 0.6, 0.8, 1.0, 1.2, 1.4, 1.6, 1.8, 2.0$ Hz
Heave amplitude	$h_0 = 0.025, 0.0375, 0.05$ m

a mirror set at 45° to the horizontal plane using a high-speed camera (Photron UX100 high-speed camera; 1280 × 1024 pixel resolution, Photron, Inc.) shooting at a frame rate of 1000 Hz. The water was seeded with near-neutral density particles that were illuminated with a 5 W argon ion laser light sheet positioned mid-span on the foils (supplemental figure 3). After masking the shadows that were caused by foils blocking the laser sheet, we calculated the flow field in each frame (two passes, 48 × 48 pixel interrogation area, DaVis v 8.3.1 LaVision, Goettingen, Germany). We subtracted the free-stream flow from the entire frame to better visualize the added effect of the foil on the fluid flow and then plotted the vorticity of the flow field in each frame. We completed this process for one cycle at each parameter combination, starting and ending with the time when the leading edge of the foil reaches maximal lateral excursion to the right, and compared the flow to CFD results at 270° phase offset.

3. Results

3.1. CFD simulation of caudal fin motion

We prescribed the heave motion of the body and the pitch motion of the caudal fin at the leading edges of both sections, allowing us to examine the energetic consequences of undulatory swimming across the full range of kinematic profiles that can be achieved by altering the relative timing of heave and pitch motions. We provide illustrations and descriptions of four representative foil profiles and one yellowfin tuna profile (figure 5) to demonstrate the range of observed motions as they compare to biological systems. When the heave and pitch are in phase ($\phi = 0°$), the caudal fin appears to be pitching about a point anterior to the tail. With a phase angle of $\phi = 90°$, the trailing edge of the caudal fin appears to lead to the motion of the whole tail. At $\phi = 180°$ the kinematic pattern was similar to the in-phase motion pattern; however, the caudal fin rotated about a point posterior to the tail. Finally, $\phi = 270°$ provided the most biomimetic kinematic profile compared to the tuna, with the caudal fin appearing to passively deflect in response to fluid resistance during lateral motions of the tail.

We find that, in addition to being the most qualitatively fish-like, a phase offset angle of $\phi = 270°$ also corresponded to an energetic optimum across all flow speeds (figure 6). Specifically, we find that the power consumption is minimized between $\phi = 180°$–$270°$, the motion patterns in which pitching of the caudal fin lags the lateral motion of the whole tail (figure 6(A)). The highest power consumption is observed around $\phi = 0°$, where the pitching of the caudal fin actively opposes the fluid resistance caused by the lateral motion of the tail. Additionally, we find that thrust is maximized when $\phi = 270°$–$360°$ and minimized when $\phi = 90°$–$180°$ (figure 6(B)). Interestingly, this means that the ranges of minimum power and maximum thrust overlap at $\phi = 270°$. Since efficient locomotion is defined as creating high thrust while consuming little power, we see a peak in Froude efficiency at $\phi = 270°$ (figure 6(C)), the motion pattern that most resembles natural undulatory locomotion. Therefore, we conclude that biomimetic kinematic profiles exist at a trade-off point between maximizing thrust and minimizing power, and that changes to the relative timing of pitch and heave could have neutral or negative consequences on swimming performance.

Given that lift is a significant source of thrust in many undulatory swimmers, we next examine the maximum angle of attack achieved during each of the tested kinematic profiles. Maxima were taken from traces of the angle of attack over one complete flapping cycle (supplemental figure 4). We find that the maximum angle of attack shows opposite trends compared to the coefficient of thrust (figure 6(D)), meaning that the highest thrust values are achieved when the foils maintain a lower angle of attack. Accordingly, we find a negative relationship between efficiency and angle of attack (figure 7). However, the degree to which efficiency is reduced at high maximum angle of attack is dependent on the phase offset angle, further highlighting the sensitivity of biomimetic motion patterns to the exact phasing of the tail and caudal fin. Furthermore, our finding of reduced thrust and efficiency at high angles of attack implies that many of these motion patterns exceed the stall angle of the fin for much of their duty cycle.

Finally, we compare our simulations to classical assumptions about optimal Strouhal numbers in swimming dynamics. We find that at certain motion parameters our model does swim in the optimal range of $0.2 < \mathrm{St} < 0.4$ (figure 8). However, this range includes both the least efficient ($\phi = 180°$, all flow speeds) and the most efficient ($\phi = 270°$, $U_\infty = 0.16$ m s^{-1}) parameter combinations. Furthermore, many of our most efficient trials had Strouhal numbers above this range. This result shows that it is possible to have highly inefficient swimming

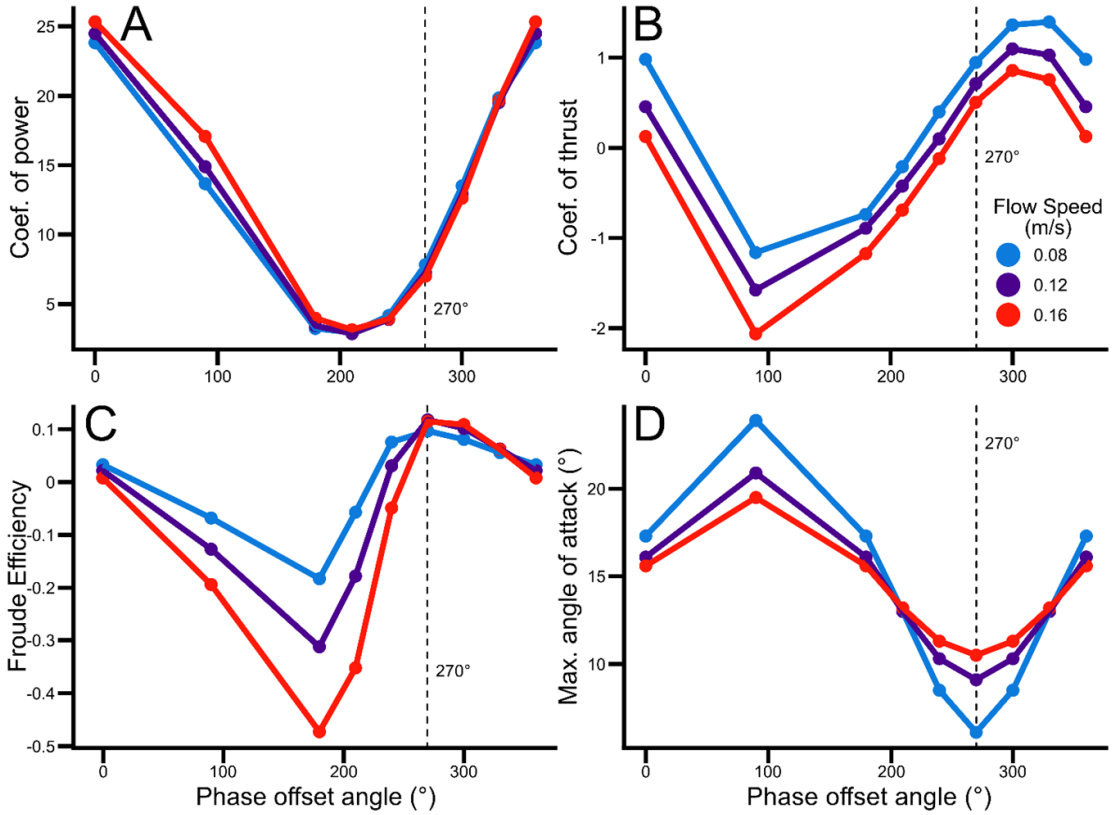

Figure 6. Across all CFD-simulated flow speeds, phase offsets near 270° nearly minimize the coefficient of power (A) and nearly maximize the coefficient of thrust (B), giving them the highest values of Froude efficiency (C). This peak in efficiency around 270° corresponds to lower maximum angles of attack (D). Color indicates flow speed in m s^{-1}.

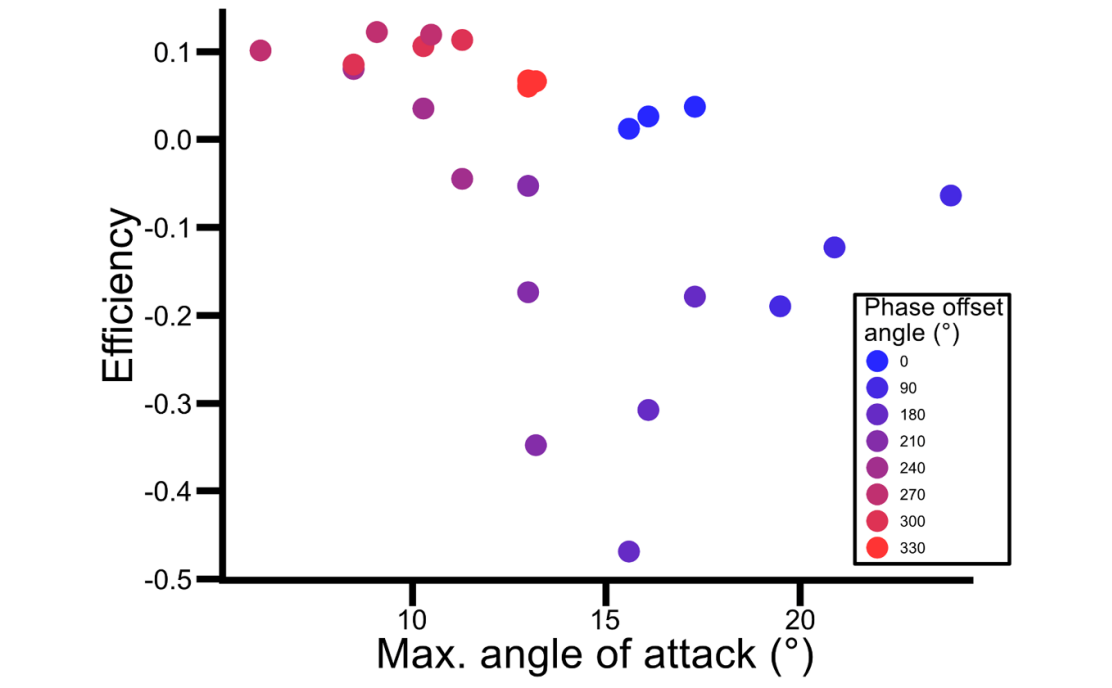

Figure 7. Efficiency and the maximum angle of attack are negatively correlated over the complete parameter space. However, the strength of the negative correlation between these two variables depends on the phase offset. In particular, very low phase offset values have a high maximum angle of attack but are only slightly less efficient than data points with a low maximum angle of attack. Mid-range phase offsets (180°–240°) show a more precipitous drop in efficiency as maximum angle of attack increases.

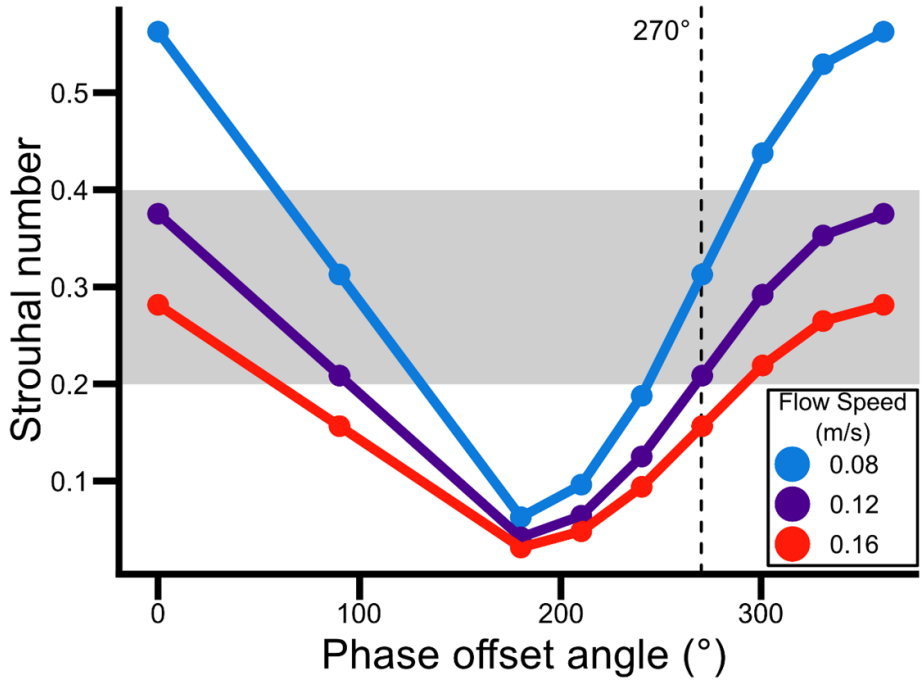

Figure 8. CFD-simulated foils covered a range of Strouhal number (St) centered around the optimal range of $0.2 < St < 0.4$ (gray). Simulations at 0.08 and 0.12 m s^{-1} with a biomimetic phase offset angle (270°) fell within this range, while the biomimetic simulation at 0.16 m s^{-1} did not.

within the range of $0.2 < St < 0.4$ if we move outside the motion patterns typically seen in undulatory swimming.

3.2. Experimental analysis of caudal fin motion

Kinematic profiles show that experimental foils are capable of being kinematically similar to CFD motion patterns at $\phi = 270°$ (figure 9(A)). Since heave is fully prescribed in both simulations and experiments, it is synchronized between the two cases. The heave amplitude of the experimental model is twice that of the simulation case to account for the increased scale of the foil. Contrastingly, the pitch is prescribed in simulations but determined by the kinematic profile and peduncle stiffness in experiments. Despite this difference, we find that the motion of experimental foils in some cases is very similar to the prescribed simulation motion, for instance when foil S3 (see table 2) is actuated at a heave of 2.5 cm and frequency of 1 Hz (tables 1 and 2; figure 9(A)). We also observe that data from flow visualization showed considerable similarities between the experimental and computational cases, with all the same major vortical structures present in both (figure 9(B)). Taken together, the similarity between foil kinematics and fluid flow confirms that simulation cases with $\phi = 270°$ are representative of passive peduncle kinematics. It also suggests that experimental results can be used to extend our understanding of the simulation efficiency peak seen at $\phi = 270°$ by elucidating the effect of peduncle stiffness on motion parameters near this phase-offset value.

We next consider the effect of peduncle stiffness on the energetics of swimming in experimental foils. Except for foil S1 (table 2), the foil with the most flexible peduncle, power consumption was similar between all our foils across all flapping frequencies (figure 10). Foil S1 consistently had higher power consumption than other tested foils, with the difference increasing at higher frequencies. Thrust production showed much more variability between foils; however, there were no clear trends where one foil was always above or below the others. Instead, we found that as the prescribed heave and frequency varied, thrust production in all the foils changed quickly. For instance, foil S1 tended to generate relatively little thrust at low frequencies, but had an inflection point at 1.4 Hz after which there was a sharp increase in the slope of thrust coefficient vs. frequency. As a result, this foil had the lowest coefficient of thrust at low frequencies and the highest coefficient of thrust at high frequencies when the heave was 3.75 cm. Although the pattern of thrust compared to frequency was similar when the heave was 2.5 and 5.0 cm, neither case had a single foil producing both the minimum and maximum values observed over the whole range of frequencies. Similarly, we observed that the foil with the highest efficiency is highly variable across different values of heave and frequency, with each foil having the highest efficiency for at least one kinematic profile. This complex set of interactions demonstrates how the relationship between peduncle stiffness and performance is highly dependent on the kinematic parameters of the tail.

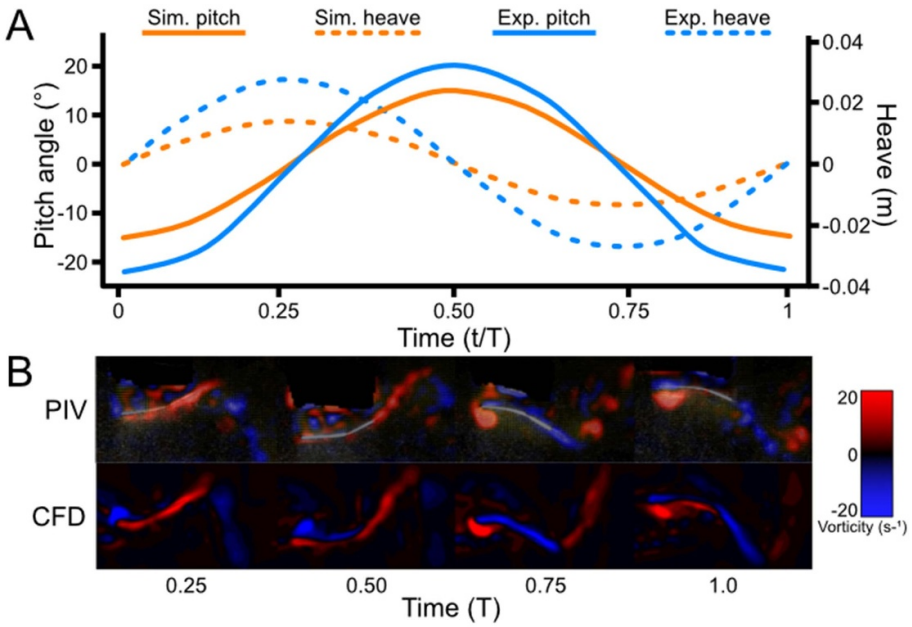

Figure 9. Both the motion of the foils (panel (A)) and of the fluid (panel (A)) are similar between simulations at 270° phase and flow tank experiments. (A) Kinematic comparison between flow tank experiments and CFD simulations at 270° phase offset angle: both pitch (left axis) and heave (right axis) motions are shown for CFD simulations and experimental data. (B) Experimental flow visualization of chordwise vorticity at four times during one tail beat cycle for foil S3 (0.07 cm peduncle thickness; table 2) at $h = 2.5$ cm and $f = 1$ Hz. CFD flow estimation from when the phase offset is 270° and flow velocity is 0.12 m s^{-1}. Mean free-stream flow has been subtracted to allow comparison between CFD and experimental data.

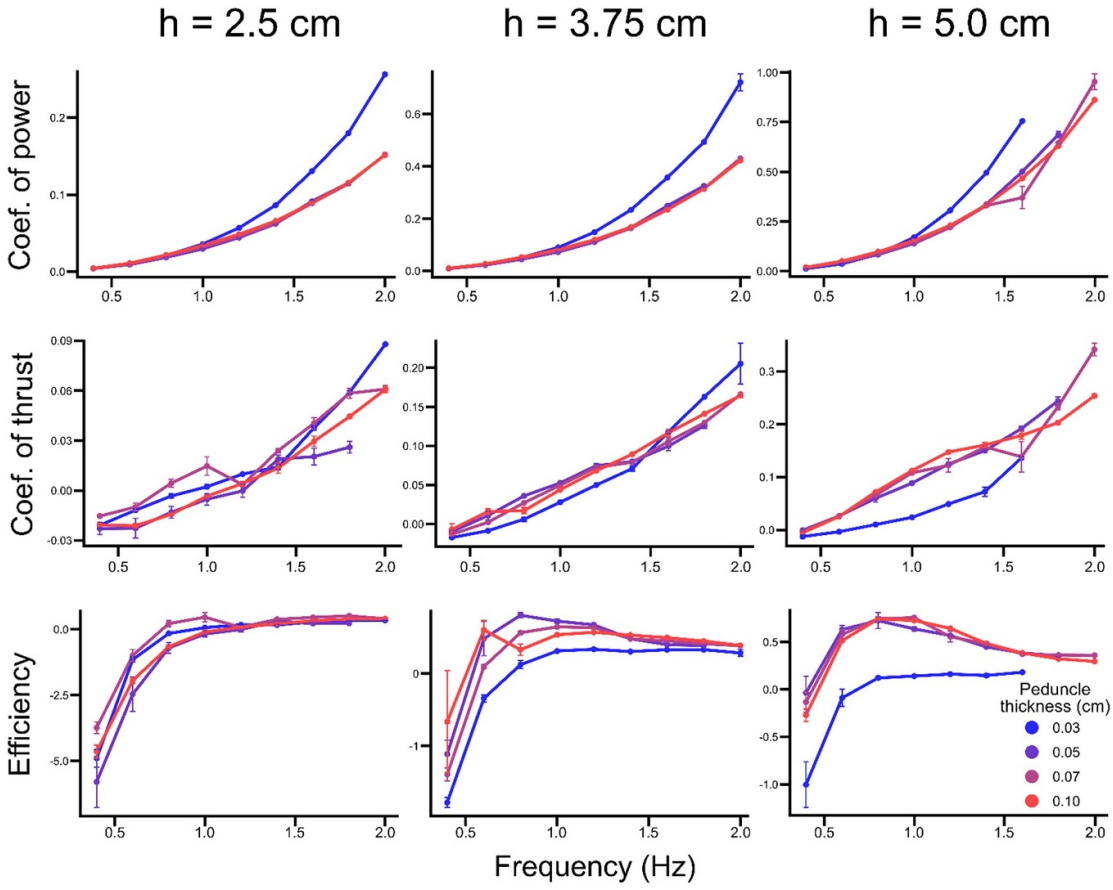

Figure 10. Experimental data on the relationships between frequency and thrust, power and efficiency for four experimental tail-shaped foils (table 2). How thrust, power and efficiency vary with frequency depends on peduncle stiffness as well as heave amplitude. Error bars represent 95% confidence intervals. Colors correspond to foils with different peduncle stiffnesses (see table 2).

4. Discussion

The caudal peduncle region just anterior to the tail in fish is an important part of their locomotor anatomy [11, 12, 47, 48] and has increasingly been incorporated into both the design of aquatic robots [1, 13, 44, 49] and the computational analyses of tuna-inspired locomotion [27, 33]. The peduncle is capable of modulating the timing and amplitude of caudal fin pitching motions and can also be used to stiffen the whole tail due to the actuation of tendons from the body musculature [1, 14, 50, 51]. As a result of the complexity of the peduncle's multifaceted effects on swimming kinematics, we do not fully understand which of these capabilities are used in fish and which ones could be beneficial in robotic design. In this paper, we use both simulations and flow tank experiments to test the energetic effects of peduncle-mediated changes on pitching and tail stiffness. We predict that the ability to phase-advance pitching of the tail will not significantly increase performance, but that the accompanying changes to the angle of attack will alter thrust production. We believe that these results will help shape our understanding of the behaviors that we see in fish and can help to optimize the design of future high-performance fish-inspired robotic models.

4.1. Efficient foil propulsion

The experimental study of flapping foil propulsion has provided numerous insights into which input motion parameters generate the most efficient undulatory movement. Many of these papers have used rigid flat plates that are oscillated in either heave, pitch, or both [23, 52, 53]. Other studies have focused on flexible foil propulsion, using simple passively bending polymeric representations of the fish body and tail moved in heave and/or pitch at the leading edge [46, 54, 55] to generate an undulatory propulsive wave down the foil. Much of this previous work has involved foils with uniform material properties along their length, as have recent computational studies of flapping foil propulsion [56].

However, given the importance of the caudal peduncle region to fish functional design and propulsion (figure 1; [1, 12, 14]), a recent trend in biomimetic swimming robots is to include a caudal peduncle in the design, often building actuation mechanisms into the peduncle itself [13, 14, 49]. Although these experiments have helped to expand the performance space that swimming robots can achieve, designing and actuating a mechanical caudal peduncle region also adds a great deal of complexity to robot design and manufacture. Therefore, it is important to understand which components of active control are highly beneficial for swimming and which benefits can be passively achieved through a simple design.

In this paper, we used a simple alteration of flexural stiffness at the base of the tail in the peduncle region (see supplemental figures 1 and 3) to determine the effect of altering the ability of the tail surface to move out of phase with the actuated anterior section on propulsive thrust and efficiency. Both computational fluid dynamics modeling and experimental studies of a flexible foil showed that passive bending at the peduncle joint was more efficient than any active phase advanced or lagged motion pattern. Specifically, power consumption was nearly minimized and thrust production was nearly maximized at the kinematic pattern where $\phi = 270°$, which is reminiscent of passive peduncle bending (figure 6). For phase-offset values $\phi < 270°$, the thrust production was much lower, while the power consumption was marginally lower. Conversely, for values $\phi > 270°$, the foils saw small increases in thrust production accompanied by large increases in power consumption. Therefore, the best motion pattern to achieve high thrust while consuming relatively little power is when $\phi = 270°$ and can be achieved with a passively actuated peduncle. However, if an application requires maximum thrust and allows for higher power consumption, then a design with active peduncle control that allows for phase lag in the caudal fin might be acceptable. Similar optimal kinematic or shape parameters have been found in cases of simple 2D geometry and low Reynolds number laminar flow conditions [23, 57, 58]. This study extends these results by examining the optimal kinematics of complex 3D systems under turbulent flow, which is only currently feasible using an experimental approach. More advanced optimization methods for 3D turbulent systems will allow for further examination of the optimal parameter spaces that fish and biomimetic robots may occupy.

We also found that the ability to actively control the stiffness of the caudal peduncle region would likely optimize performance across a range of swimming parameters and behaviors. Unlike the phase-lag experiments, there is no single peduncle stiffness value at which maximum performance is achieved across the range of experimental parameters (figure 10). Instead, we found that each set of parameters had a different optimal peduncle stiffness value. In addition, the optimal stiffness value that maximizes efficiency was often different from that which would optimize thrust or minimize power consumption. Therefore, optimizing performance across a range of behaviors requires active alteration of peduncle stiffness during swimming. This strategy has been explored by Zhong *et al* [14], and our results indicate that other studies could benefit from similar mechanisms.

Although a great deal of fish swimming performance is determined by the tail, it is also important to remember that drag and wake structure

from the body and other fins also have an important role in swimming dynamics. Specifically, more anterior median fins can leave vortical structures that alter the angle of attack over the caudal fin [33, 34, 43, 49, 59–61]. The foils used in this study only represented the posterior region of fish, and therefore lacked any other median fins. Although this was necessary to ensure that our results pertained specifically to peduncle mediated effects, it also means that some of the performance trade-offs in our model could be avoided in more complicated models by using structures on the anterior body to alter the flow environment that the tail encounters [49], such as changing lateral flow momentum through median fins.

4.2. Implications for fish propulsion

In addition to guiding robotic design, our results also allow us to better understand how fish use their complex anatomy to control swimming performance. Specifically, in regard to the peduncle, fish have passive anatomical structures that impact the stiffness of the tail (figure 1(C)) [11, 12, 50] as well as active control of the muscles and tendons that span the peduncle. This active control grants them the ability to both phase shift the motion of the caudal fin relative to the body and to actively stiffen the peduncle. We believe that phase shifting the caudal fin is unlikely to be advantageous in steady swimming since our results show that efficiency quickly decreases outside the passive range of phase-shift angles. However, our finding that the performance of a passively deflecting peduncle is dependent on stiffness and is sensitive to tail kinematics leads us to believe that fish would benefit from active modulation of peduncle stiffness as shown in a robotic model by Zhong *et al* [14].

Throughout their lives, fish exhibit a huge range of behaviors that necessitate swimming over a broad range of speeds and with a wide variety of body kinematics. While the passive stiffness granted by the anatomy of the peduncle may lead to effective locomotion in one context, our results suggest that it would likely be suboptimal in other contexts. By activating the muscles and tendons that span the peduncle, fish could increase peduncle stiffness and maintain effective propulsion across a variety of behaviors [1, 9]. Specifically, this could allow fish to alter the deflection of the caudal fin as the tail moves laterally, thereby changing the angle of attack of the fin. Since performance variation was low between adjacent frequencies in our trials, we predict that fish change the stiffness of the peduncle only for major changes to swimming behavior, instead of fine-tuning stiffness during each tailbeat. However, electrophysiological examination of the peduncle muscles is needed to definitively understand the degree to which fish actively modulate peduncle stiffness.

5. Conclusion

We present a study that combines simulations and robotic experiments to demonstrate the importance of the caudal peduncle in swimming performance using a simplified model of the posterior region of a fish's body. Simulation results suggest that there is a tradeoff between thrust and power consumption in undulatory swimming systems. They furthermore show that biomimetic values of the phase lag between tail heave and pitch lead to the best balance of these two performance metrics. Experiments of peduncle stiffness show that although there are optimal values of joint stiffness for individual kinematic profiles, there is no optimal global solution to maximize any measure of performance. Our results demonstrate that optimization can be achieved by incorporating fish-like caudal peduncles into the design of undulatory swimming systems and stress the importance of future research on actively controlled stiffness in both peduncle joints and other parts of the body.

Data availability statement

The data that support the findings of this study are openly available at the following URL/DOI: https://dataverse.harvard.edu/dataset.xhtml?persistentId=doi:10.7910/DVN/UAGRFJ.

Acknowledgments

We thank the members of the Bart-Smith, Dong, and Lauder labs for many fruitful discussions, and Professor Dan Quinn for his collaborative work on fish and robot body stiffness.

Conflict of interest

The authors declare that there is no conflict of interest.

Funding

This project was supported by the Office of Naval Research Grant Nos. N00014-21-1-2210, N000141410533, and N00014-15-1-2234, and NSF No. Grant 093088-17158 to G V L, NSF graduate research fellowship under Grant No. DGE1745303 to D G M, School of Engineering and Applied Science Distinguished Fellowship of the University of Virginia to J W, and ONR Grant No. N00014-21-1-2210 to H B-S and H D.

Ethical statement

No animals were used in this project. All pertinent ethical guidelines were followed.

ORCID iDs

David G Matthews https://orcid.org/0000-0002-5926-4348
Ruijie Zhu https://orcid.org/0000-0002-6859-2036
Junshi Wang https://orcid.org/0000-0002-7486-3410
Haibo Dong https://orcid.org/0000-0001-7823-7014
Hilary Bart-Smith https://orcid.org/0000-0001-7469-7734
George Lauder https://orcid.org/0000-0003-0731-286X

References

[1] Quinn D and Lauder G 2022 Tunable stiffness in fish robotics: mechanisms and advantages *Bioinspir. Biomim.* **17** 011002
[2] Long J H, Mchenry M J and Boetticher N C 1994 Undulatory swimming: how traveling waves are produced and modulated in sunfish *J. Exp. Biol.* **192** 129–45
[3] Tytell E D, Hsu C-Y and Fauci L J 2014 The role of mechanical resonance in the neural control of swimming in fishes *Zoology* **117** 48–56
[4] Tytell E D, Leftwich M C, Hsu C-Y, Griffith B E, Cohen A H, Smits A J, Hamlet C and Fauci L J 2016 Role of body stiffness in undulatory swimming: insights from robotic and computational models *Phys. Rev. Fluids* **1** 073202
[5] Long J H and Nipper K S 1996 The importance of body stiffness in undulatory propulsion *Am. Zool.* **36** 678–94
[6] Alben S, Madden P G and Lauder G V 2007 The mechanics of active fin-shape control in ray-finned fishes *J. R. Soc. Interface* **4** 243–56
[7] Flammang B E, Alben S, Madden P G A and Lauder G V 2013 Functional morphology of the fin rays of teleost fishes: functional morphology of fish fin rays *J. Morphol.* **274** 1044–59
[8] Lauder G V, Madden P G A, Tangorra J L, Anderson E and Baker T V 2011 Bioinspiration from fish for smart material design and function *Smart Mater. Struct.* **20** 094014
[9] Flammang B E and Lauder G V 2008 Speed-dependent intrinsic caudal fin muscle recruitment during steady swimming in bluegill sunfish, *Lepomis macrochirus J. Exp. Biol.* **211** 587–98
[10] Flammang B E and Lauder G V 2009 Caudal fin shape modulation and control during acceleration, braking and backing maneuvers in bluegill sunfish, *Lepomis macrochirus J. Exp. Biol.* **212** 277–86
[11] Fierstine H L and Walters V 1968 Studies in locomotion and anatomy of scombroid fishes *Mem. South. Calif. Acad. Sci.* **6** 1–31
[12] Wainwright D K and Lauder G V 2020 Tunas as a high-performance fish platform for inspiring the next generation of autonomous underwater vehicles *Bioinspir. Biomim.* **15** 035007
[13] Ren Z, Yang X, Wang T and Wen L 2016 Hydrodynamics of a robotic fish tail: effects of the caudal peduncle, fin ray motions and the flow speed *Bioinspir. Biomim.* **11** 016008
[14] Zhong Q, Zhu J, Fish F E, Kerr S J, Downs A M, Bart-Smith H and Quinn D B 2021 Tunable stiffness enables fast and efficient swimming in fish-like robots *Sci. Robot.* **6** eabe4088
[15] Zhu J, White C, Wainwright D K, Di Santo V, Lauder G V and Bart-Smith H 2019 Tuna robotics: a high-frequency experimental platform exploring the performance space of swimming fishes *Sci. Robot.* **4** eaax4615
[16] White C H, Lauder G V and Bart-Smith H 2021 Tunabot flex: a tuna-inspired robot with body flexibility improves high-performance swimming *Bioinspir. Biomim.* **16** 026019
[17] Jayne B C and Lauder G V 1995 Speed effects on midline kinematics during steady undulatory swimming of largemouth bass, *Micropterus salmoides J. Exp. Biol.* **195** 585–602
[18] Jayne J and Lauder L 1995 Red muscle motor patterns during steady swimming in largemouth bass: effects of speed and correlations with axial kinematics *J. Exp. Biol.* **198** 1575–87
[19] Shadwick R E and Gemballa S 2005 Structure, kinematics, and muscle dynamics in undulatory swimming *Fish Physiol.* **23** 241–80
[20] Vogel S 1994 *Life in Moving Fluids: The Physical Biology of Flow* 2nd edn (Princeton, NJ: Princeton University Press)
[21] Walker J A and Westneat M W 2000 Mechanical performance of aquatic rowing and flying *Proc. R. Soc.* B **267** 1875–81
[22] Walker J A and Westneat M W 2002 Kinematics, dynamics, and energetics of rowing and flapping propulsion in fishes *Integr. Comp. Biol.* **42** 1032–43
[23] Van Buren T, Floryan D and Smits A J 2019 Scaling and performance of simultaneously heaving and pitching foils *AIAA J.* **57** 3666–77
[24] Moriche M, Flores O and García-Villalba M 2017 On the aerodynamic forces on heaving and pitching airfoils at low Reynolds number *J. Fluid Mech.* **828** 395–423
[25] Mittal R, Dong H, Bozkurttas M, Najjar F M, Vargas A and von Loebbecke A 2008 A versatile sharp interface immersed boundary method for incompressible flows with complex boundaries *J. Comput. Phys.* **227** 4825–52
[26] Sin F S, Schroeder D and Barbič J 2013 Vega: non-linear FEM deformable object simulator *Comput. Graph. Forum* **32** 36–48
[27] Wang J, Lauder G and Dong H 2022 Effect of tunable stiffness on the hydrodynamic performance of a tuna tail informed flexible propulsor *AIAA SCITECH 2022 Forum* (San Diego, CA: American Institute of Aeronautics and Astronautics) (https://doi.org/10.2514/6.2022-0729)
[28] Liu G, Dong H and Li C 2016 Vortex dynamics and new lift enhancement mechanism of wing–body interaction in insect forward flight *J. Fluid Mech.* **795** 634–51
[29] Bode-Oke A T, Zeyghami S and Dong H 2018 Flying in reverse: kinematics and aerodynamics of a dragonfly in backward free flight *J. R. Soc. Interface* **15** 20180102
[30] Li C, Wang J and Dong H 2017 Proper orthogonal decomposition analysis of flapping hovering wings *55th AIAA Aerospace Sciences Meeting* (Grapevine, TX: American Institute of Aeronautics and Astronautics) (https://doi.org/10.2514/6.2017-0327)
[31] Ren Y, Dong H, Deng X and Tobalske B 2016 Turning on a dime: asymmetric vortex formation in hummingbird maneuvering flight *Phys. Rev. Fluids* **1** 050511
[32] Wang J, Ren Y, Li C and Dong H 2019 Computational investigation of wing-body interaction and its lift enhancement effect in hummingbird forward flight *Bioinspir. Biomim.* **14** 046010
[33] Wang J, Wainwright D K, Lindengren R E, Lauder G V and Dong H 2020 Tuna locomotion: a computational hydrodynamic analysis of finlet function *J. R. Soc. Interface* **17** 20190590
[34] Han P, Lauder G V and Dong H 2020 Hydrodynamics of median-fin interactions in fish-like locomotion: effects of fin shape and movement *Phys. Fluids* **32** 011902
[35] Liu G, Ren Y, Zhu J, Bart-Smith H and Dong H 2015 Thrust producing mechanisms in ray-inspired underwater vehicle propulsion *Theor. Appl. Mech. Lett.* **5** 54–57
[36] Pan Y and Dong H 2020 Computational analysis of hydrodynamic interactions in a high-density fish school *Phys. Fluids* **32** 121901

[37] Werner N H, Chung H, Wang J, Liu G, Cimbala J M, Dong H and Cheng B 2019 Radial planetary vorticity tilting in the leading-edge vortex of revolving wings *Phys. Fluids* **31** 041902
[38] Wang J, Xi J, Han P, Wongwiset N, Pontius J and Dong H 2019 Computational analysis of a flapping uvula on aerodynamics and pharyngeal wall collapsibility in sleep apnea *J. Biomech.* **94** 88–98
[39] Dong H, Mittal R and Najjar F M 2006 Wake topology and hydrodynamic performance of low-aspect-ratio flapping foils *J. Fluid Mech.* **566** 309
[40] Li C, Dong H and Liu G 2015 Effects of a dynamic trailing-edge flap on the aerodynamic performance and flow structures in hovering flight *J. Fluids Struct.* **58** 49–65
[41] Wang J, Deng X, Lauder G V and Dong H 2019 Numerical investigation on hydrodynamic performance of flapping plates with non-uniform spanwise flexibility using fluid structure interaction *AIAA Aviation 2019 Forum* (Dallas, TX: American Institute of Aeronautics and Astronautics) (https://doi.org/10.2514/6.2019-3434)
[42] Domel A G, Domel G, Weaver J C, Saadat M, Bertoldi K and Lauder G V 2018 Hydrodynamic properties of biomimetic shark skin: effect of denticle size and swimming speed *Bioinspir. Biomim.* **13** 056014
[43] Matthews D G and Lauder G V 2021 Fin–fin interactions during locomotion in a simplified biomimetic fish model *Bioinspir. Biomim.* **16** 046023
[44] Quinn D B, Lauder G V and Smits A J 2015 Maximizing the efficiency of a flexible propulsor using experimental optimization *J. Fluid Mech.* **767** 430–48
[45] Saadat M, Fish F E, Domel A G, Di Santo V, Lauder G V and Haj-Hariri H 2017 On the rules for aquatic locomotion *Phys. Rev. Fluids* **2** 083102
[46] Shelton R M, Thornycroft P J M and Lauder G V 2014 Undulatory locomotion of flexible foils as biomimetic models for understanding fish propulsion *J. Exp. Biol.* **217** 2110–20
[47] Nauen J C and Lauder G V 2001 Locomotion in scombrid fishes: visualization of flow around the caudal peduncle and finlets of the chub mackerel *Scomber japonicus J. Exp. Biol.* **204** 2251–63
[48] Webb P W 1982 Locomotor patterns in the evolution of actinopterygian fishes *Am. Zool.* **22** 329–42
[49] Mignano A, Kadapa S, Tangorra J and Lauder G 2019 Passing the wake: using multiple fins to shape forces for swimming *Biomimetics* **4** 23
[50] Westneat M W and Wainwright S A 2001 Mechanical design for swimming: muscle, tendon, and bone *Fish Physiol.* **19** 271–311
[51] Westneat M W, Hoese W, Pell C A and Wainwright S A 1993 The horizontal septum: mechanisms of force transfer in locomotion of scombrid fishes (Scombridae, Perciformes) *J. Morphol.* **217** 183–204
[52] Floryan D, Van Buren T, Rowley C W and Smits A J 2017 Scaling the propulsive performance of heaving and pitching foils *J. Fluid Mech.* **822** 386–97
[53] Smits A J 2019 Undulatory and oscillatory swimming *J. Fluid Mech.* **874** P1
[54] Alben S, Witt C, Baker T V, Anderson E and Lauder G V 2012 Dynamics of freely swimming flexible foils *Phys. Fluids* **24** 051901
[55] Lauder G V, Flammang B and Alben S 2012 Passive robotic models of propulsion by the bodies and caudal fins of fish *Integr. Comp. Biol.* **52** 576–87
[56] Paniccia D, Padovani L, Graziani G and Piva R 2021 The performance of a flapping foil for a self-propelled fishlike body *Sci. Rep.* **11** 22297
[57] Kaya M and Tuncer I H 2007 Nonsinusoidal path optimization of a flapping airfoil *AIAA J.* **45** 2075–82
[58] Read D A, Hover F S and Triantafyllou M S 2003 Forces on oscillating foils for propulsion and maneuvering *J. Fluids Struct.* **17** 163–83
[59] Liu G, Ren Y, Dong H, Akanyeti O, Liao J C and Lauder G V 2017 Computational analysis of vortex dynamics and performance enhancement due to body–fin and fin–fin interactions in fish-like locomotion *J. Fluid Mech.* **829** 65–88
[60] Zhong Q, Dong H and Quinn D B 2019 How dorsal fin sharpness affects swimming speed and economy *J. Fluid Mech.* **878** 370–85
[61] Drucker E G and Lauder G V 2001 Locomotor function of the dorsal fin in teleost fishes: experimental analysis of wake forces in sunfish *J. Exp. Biol.* **204** 2943–58